


Article

PARP Inhibition Increases the Response to Chemotherapy in Uveal Melanoma

Leanne de Koning ^{1,*†}, Didier Decaudin ^{2,3,*†}, Rania El Botty ², André Nicolas ⁴, Guillaume Carita ², Mathieu Schuller ², Bérengère Ouine ¹, Aurélie Cartier ¹, Adnan Naguez ², Justine Fleury ², Vesselina Cooke ⁵, Andrew Wylie ⁵, Paul Smith ⁶, Elisabetta Marangoni ², David Gentien ⁷ , Didier Meseure ⁴, Pascale Mariani ⁸, Nathalie Cassoux ⁹, Sophie Piperno-Neumann ³, Sergio Roman-Roman ¹⁰ and Fariba Némati ²

¹ RPPA Platform, Department of Translational Research, Institut Curie, PSL University, 75248 Paris, France; berengere.ouine@curie.fr (B.O.); aurelie.cartier10@laposte.net (A.C.)

² Laboratory of Preclinical Investigation, Department of Translational Research, Institut Curie, PSL University, 75248 Paris, France; rania.el-botty@curie.fr (R.E.B.); guillaume.carita@gmail.com (G.C.); mathieu.schuller@curie.fr (M.S.); adnan.naguez@curie.fr (A.N.); justine.fleury04@gmail.com (J.F.); elisabetta.marangoni@curie.fr (E.M.); fariba.nemati@curie.fr (F.N.)

³ Department of Medical Oncology, Institut Curie, 75248 Paris, France; sophie.piperno-neumann@curie.fr

⁴ Department of Tumor Biology, Institut Curie, 75248 Paris, France; andre.nicolas@curie.fr (A.N.); didier.meseure@curie.fr (D.M.)

⁵ Novartis Institutes for BioMedical Research, Translational Clinical Oncology, Cambridge, MA 02139, USA; vesselina.cooke@novartis.com (V.C.); andrew.wylie@novartis.com (A.W.)

⁶ Oncology IMED, AstraZeneca, 1 Francis Crick Avenue, Cambridge Biomedical Campus, Cambridge CB2 0AA, UK; paul.smith@astra-zeneca.com

⁷ Genomics Platform, Department of Translational Research, Institut Curie, PSL University, 75248 Paris, France; david.gentien@curie.fr

⁸ Department of Surgery, Institut Curie, 75248 Paris, France; pascale.mariani@curie.fr

⁹ Department of Ophthalmologic Surgery, Institut Curie, University of Medicine René Descartes Paris V, 75248 Paris, France; nathalie.cassoux@curie.fr

¹⁰ Department of Translational Research, Institut Curie, PSL University, 75248 Paris, France; sergio.roman-roman@curie.fr

* Correspondence: leanne.de-koning@curie.fr (L.d.K.); didier.decaudin@curie.fr (D.D.); Tel.: +33-1-5624-6285 (L.d.K.); +33-1-5624-6240 (D.D.)

† These two authors have contributed equally to this work.

Received: 13 March 2019; Accepted: 27 May 2019; Published: 29 May 2019



Abstract: Uveal melanoma (UM) remains without effective therapy at the metastatic stage, which is associated with *BAP-1* (BRCA1 associated protein) mutations. However, no data on DNA repair capacities in UM are available. Here, we use UM patient-derived xenografts (PDXs) to study the therapeutic activity of the PARP inhibitor olaparib, alone or in combination. First, we show that the expression and the activity of PARP proteins is similar between the PDXs and the corresponding patient's tumors. In vivo experiments in the PDX models showed that olaparib was not efficient alone, but significantly increased the efficacy of dacarbazine. Finally, using reverse phase protein arrays and immunohistochemistry, we identified proteins involved in DNA repair and apoptosis as potential biomarkers predicting response to the combination of olaparib and dacarbazine. We also observed a high increase of phosphorylated YAP and TAZ proteins after dacarbazine + olaparib treatment. Our results suggest that PARP inhibition in combination with the alkylating agent dacarbazine could be of clinical interest for UM treatment. We also observe an interesting effect of dacarbazine on the Hippo pathway, confirming the importance of this pathway in UM.

Keywords: PARP inhibitor; treatment combinations; uveal melanomas; patient-derived xenografts

1. Introduction

Uveal melanoma (UM) is a rare tumor affecting 7/1.0 million of the Western population per year [1] for which no effective systemic therapies exist at the metastatic stage. Dacarbazine (DTIC), which is an alkylating agent leading to DNA lesions, is often the standard arm in trials in metastatic UM, but response rate remains disappointing. Several studies have thus focused on the molecular characterization of UM, with the aim to identify new subpopulations or therapeutic targets [2–7]. Well-described recurrent mutations have been observed, such as the *GNAQ* or *GNA11* genes, which are mutated in about 80% of UM and lead to a constitutive activation of the MAPK (mitogen activated protein kinase) and Hippo pathways [8,9]. Nevertheless, the MEK1/2 inhibitor selumetinib, in combination with dacarbazine, fails to improve progression-free survival of metastatic UM [10]. Various targeted therapies have therefore been tested in combination with selumetinib [11] or with the PKC (protein kinase C) inhibitor AEB071 [12] in UM preclinical models, and particularly in patient-derived xenografts (PDXs). On this basis, this last compound is currently being tested in a clinical trial, currently in combination with a MDM2 inhibitor (NCT02601378).

Another recurrent mutation in UM is the *bap1* (*BRCA1-associated protein 1*) gene mutation [13], which is associated with a higher risk of metastases [14,15]. Sporadic germline *bap1* mutations confer a predisposition to several types of cancer, including UM [16], confirming its role in tumorigenesis. BAP1 is a deubiquitinating enzyme involved in chromatin structure, cell cycle progression, and differentiation. Although the direct interaction of BAP1 with BRCA1 remains controversial [17], several studies report a potential role of BAP1 in DNA damage repair, and particularly in homologous recombination (HR). BAP1 is recruited to double strand breaks (DSB) and promotes DNA repair and survival after DNA damage induction [18–20]. BAP1 recruitment would be poly(ADP-ribose) polymerase (PARP) dependent [18] and BAP1 function would be required for efficient recruitment of BRCA1 and RAD51 to DNA repair foci [19,20]. In conclusion, BAP1 deficiency might lead to impaired DSB repair by HR and could potentially increase the reliance on parallel repair pathways in a similar manner as BRCA1 deficiency.

Given the potential role of BAP-1 in DNA repair and the frequent administration of dacarbazine, it is surprising that the DNA repair pathways and their therapeutic potential have not yet been evaluated in UM. We hypothesized that PARP may be an interesting target in UM, alone or in combination with other therapies. Indeed, the PARP proteins catalyze the transfer of ADP-ribose to target proteins. PARPs play an important role in various cellular processes and notably in DNA repair by base-excision repair (BER) and nucleotide excision repair (NER). BER and NER are required for repair of DNA lesions induced by certain chemotherapeutic agents and PARP inhibition is therefore an attractive therapeutic option in combination with chemotherapy [21]. Cells displaying deficiencies in HR particularly rely on PARP and are thus remarkably sensitive to PARP inhibition [22]. Whether this could be the case in BAP-1 mutated melanoma has not been assessed. PARP expression and activity has not been extensively studied in UM. One study showed varying mRNA and protein expression levels of PARP1, as well as PARP1 enzymatic activity in five UM cell lines [23]. Similarly, in a small series of 12 UM, a slight and variable perivascular PAR staining has been observed [24]. Hence, it remains to be demonstrated whether PARP could be a therapeutic target in UM patients.

Here, we explore PARP expression in both UM patient's tumors and a unique panel of PDXs, and we evaluate for the first time the therapeutic potential of the PARP inhibitor olaparib used alone or in various combinations in UM PDXs. Next, using RPPA (reverse phase protein array), WB (western blots), and IHC (immunohistochemistry) analyses, we explored predictive factors that are implicated in the additive effect of olaparib + dacarbazine, as well as protein modifications observed in treated tumors. Hence, our study may be a pivotal preclinical study for the clinical application of PARP inhibitor in the treatment of metastatic UM patients.

2. Results

2.1. Basal Gene and Protein Expression of PARPs in Patient's Tumors and Corresponding PDXs

The expression of *PARP* family genes was evaluated using data generated from previously reported Affymetrix GeneChip-Human Exon 1.0 ST arrays, including 12 patient tumors and 32 PDXs (15 at passage one, 13 at passage four, and four at passage nine). Two control genes were used to assess positive and negative expression, i.e., the *MAGE1* gene (negative expression) and the *MGAT5* gene (positive expression). We observed variable expression levels among all *PARP* family genes, with high expression of *PARP1*, *PARP4*, *PARP6*, *PARP10*, *PARP12*, and *PARP14* genes. Moreover, we did not observe variations in gene expression levels between patient's tumors and their corresponding PDXs at three different in vivo passages (Figure 1 and Figure S1).

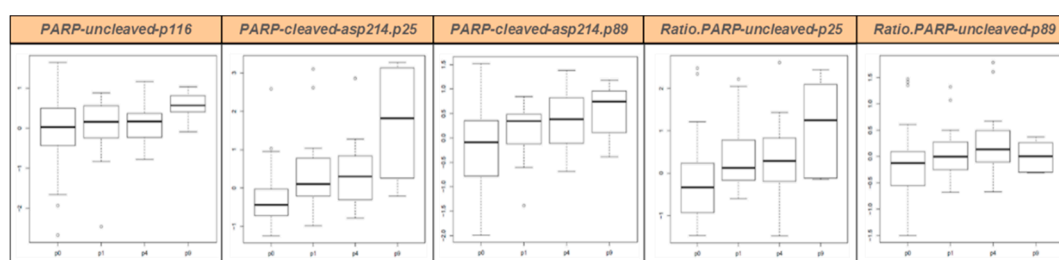


Figure 1. PARP protein expression in UM patients (P0) and their corresponding PDXs at various in vivo passages (P1, P4, and P9) as measured by RPPA. Boxplots represent the distribution of data of all PDX models together. Boxes contain 50% of values, upper brackets contain the 25% highest values, lower brackets contain the 25% lowest values. Black lines: median; dots: outliers. P0, patient's tumor; P1, first in vivo passage; P4, fourth in vivo passage; P9, ninth in vivo passage.

Similarly, we studied protein expression of the p116 uncleaved PARP, the two p25 and p89 cleavage products of PARPs, and the two corresponding ratios cleaved/uncleaved PARPs, using RPPA. Patient's tumors (P0) and corresponding PDXs at various in vivo passages (P1, P4, and P9) were studied (ten pairs P0–P1 or P0–P4, four pairs P0–P9, 13 pairs P1–P4, and six pairs P4–P9). All results are presented in Figure 1 and in Table S1. We conclude that PARP protein expression and cleavage was stable between patient's tumors and their corresponding PDXs at early in vivo passages (P1 and P4). For passage nine, only four PDXs have been studied, and results are therefore less robust, but even at this late passage little variation is visible.

2.2. Olaparib Increased DTIC Antitumor Activity in UM PDXs

Various olaparib-based combinations with chemotherapies or targeted therapies were tested in 11 unique well-characterized UM PDXs (Table S2) that were already used for pharmacological assessments [11,12,25–27] and that well reproduce patients' tumors [28,29].

First, we performed a global comparison of all tested treatments in the various sets of in vivo experiments. Indeed, olaparib was tested in ten models (137 mice); DTIC and fotemustine, which are the two main chemotherapies used in metastatic UM patients, were tested in six models (47 mice) and two models (17 mice), respectively; everolimus, AEB071, and CGM097, that have already showed preclinical efficiency in UM PDXs [12,26], were tested in one (eight mice), three (23 mice), and five (12 mice) models, respectively; finally, AZD0156 and AZD6738, both treatments that may impact DNA repair, were tested in five PDX models (14 and 16 mice, respectively). In all these experiments, as shown in Figure 2, an overall response rate (ORR) below -0.5 and -0.9 was observed in 16% and 0% of mice after olaparib; 43% and 15% after DTIC; 59% and 41% after fotemustine; 75% and 0% after everolimus; 43% and 4% after AEB071; 33% and 0% after CGM097; 20% and 0% after AZD 156; and 33% and 0% after AZD6738. In conclusion, in all tested UM PDXs, olaparib monotherapy was significantly

less efficient than DTIC ($p < 10^{-3}$), fotemustine ($p < 10^{-3}$), everolimus ($p < 10^{-3}$), and AEB071 ($p < 10^{-2}$), and no significant differences were observed between olaparib and CGM097, AZD0156, and AZD6738.

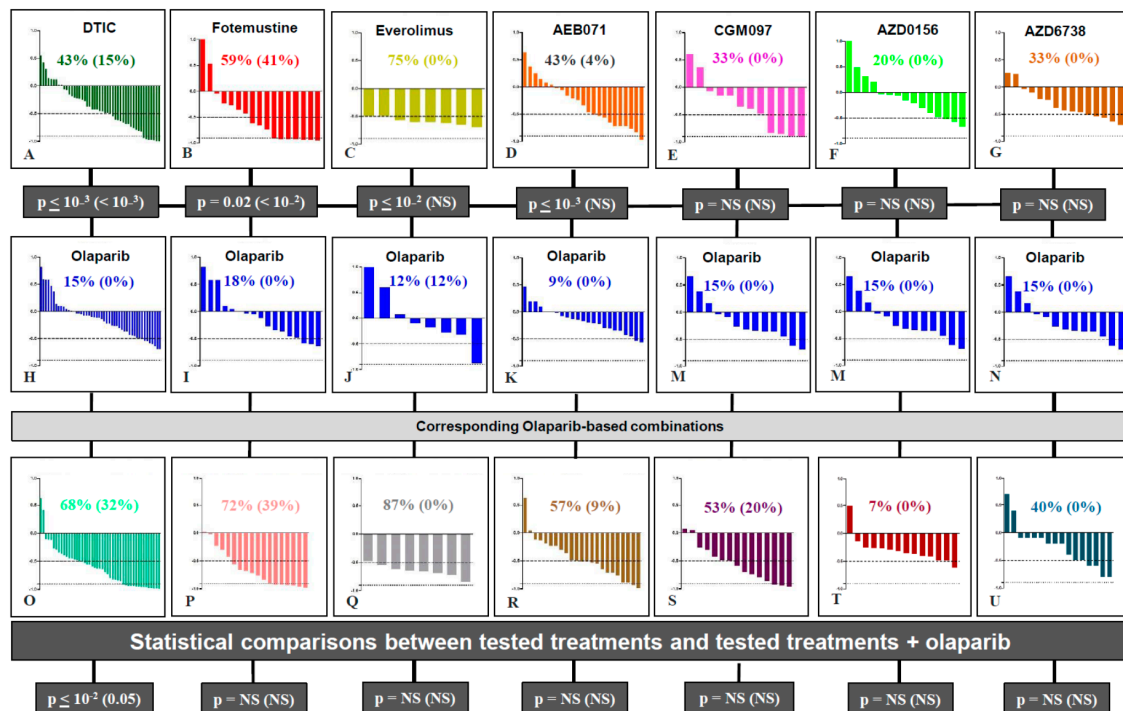


Figure 2. Waterfall plots of response to olaparib-based therapies. Upper p values correspond to statistical differences between olaparib compared to each other tested treatment; p values at the bottom correspond to statistical differences between each tested treatment compared to its combination with olaparib (χ^2 test).

We hypothesized that olaparib could have an antitumor effect when combined with other therapies and notably with DNA damaging agents, as has been described in other tumor types [30]. We therefore performed a comparison of the ORR of each olaparib-based combination (i.e., olaparib + DTIC, fotemustine, everolimus, AEB071, CGM097, AZD0156, or AZD6738) versus the corresponding compound alone (Figure 2). Only the combination of olaparib + DTIC showed a significantly improved response rate compared to DTIC monotherapy, both for an ORR lower than -0.5 and -0.9 ($p < 10^{-2}$ and 0.05 , respectively). The ORR ≤ -0.5 increased from 43% for monotherapy to 68% in the combination therapy. Similarly, the ORR ≤ -0.9 increased from 15% to 32%. Six models (MP41, MP55, MP77, MM33, MM52, and MM66) were treated with the olaparib + DTIC combination (Figure 3). For these six experiments, the median RTV of all treated mice was 10.1, 7.6, 5.6, and 1.9 for the control, olaparib, DTIC, and olaparib + DTIC groups, respectively. Similarly, the median probability of progression (doubling time) was 8, 10, 11.5, and 31 days for the control, olaparib, DTIC, and olaparib + DTIC groups, respectively. In conclusion, olaparib significantly increases the antitumor activity of DTIC in UM PDXs, as shown by an increased response rate, reduced tumor volume and prolonged doubling time. In contrast, no significant benefit was observed in other tested olaparib-based combinations (Figures S3–S8).

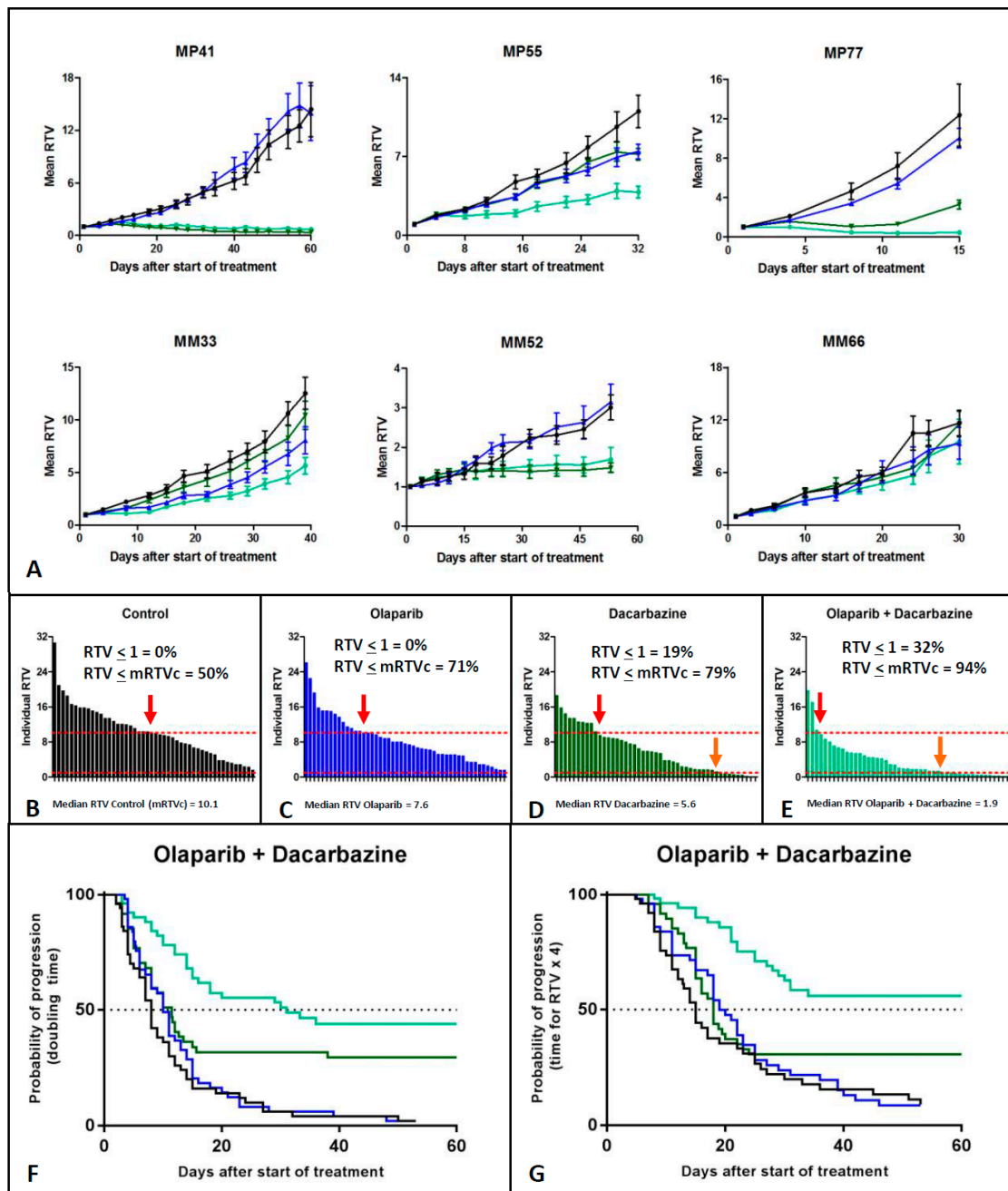


Figure 3. Combination of olaparib and dacarbazine. (A) Growth curves of all treated models. (B–E) ORR of the four experimental groups, i.e., control (black), olaparib (blue), dacarbazine (dark green), and olaparib + dacarbazine (light green), respectively. RTV: Relative tumor variation. mRTVc: median relative tumor volume of the corresponding control group (F–G). Probability of progression of the four experimental groups: doubling time (F) and quadrupling time (G).

2.3. RPPA-Based Proteomic Study of Olaparib + DTIC Combination in Four UM PDXs

The aim of the proteomic RPPA-based study was to evaluate the correlation of treatment efficacy (olaparib alone, DTIC alone, and olaparib + DTIC) with the expression and activation of various proteins, in order to identify proteins that may play a role in the additive effect of olaparib combined with DTIC. We selected proteins involved in DNA repair, apoptosis induction, and MAPK, Pi3K- and Hippo-signaling pathways. Among the six PDXs that received the olaparib + DTIC combination, four of them were included in the RPPA study, i.e., MP55, MP77, MM33, and MM52. Four to five

tumors collected at the end of in vivo experiments and under therapies were studied in each group (control, olaparib, DTIC, and olaparib + DTIC). Overall, the combination of olaparib + DTIC showed an additive effect in three models (MP55, MP77, MM33), while the fourth did not (MM52), with a total number of 15 and seven tumors in the two respective groups.

First, we aimed to define predictive protein markers for the additive efficacy of DTIC + olaparib. For this, we defined proteins whose expression are predictive for response to DTIC alone (MP55, MP77, and MM52), olaparib alone (MM33), and DTIC + olaparib (MP55, MP77, and MM33) in the untreated (control) mice. We then determined proteins that are exclusively correlated to the additive effect of the combination and not to each monotherapy (Figure 4, Figures S9 and S10). Interestingly, the main involved proteins belong to the DNA-repair function, with particularly high expression of both PARP and c-PARP proteins, as well as p-FANCD2, p-FANCD2/FANCD2, P53, p-P53, and low expression of ATM, p-ATM, and p-Topo.IIa/Topo.IIa proteins. We also underline the predictive value of low Bcl-X_L protein ($p = 5.1 \times 10^{-4}$) (Figure 4).

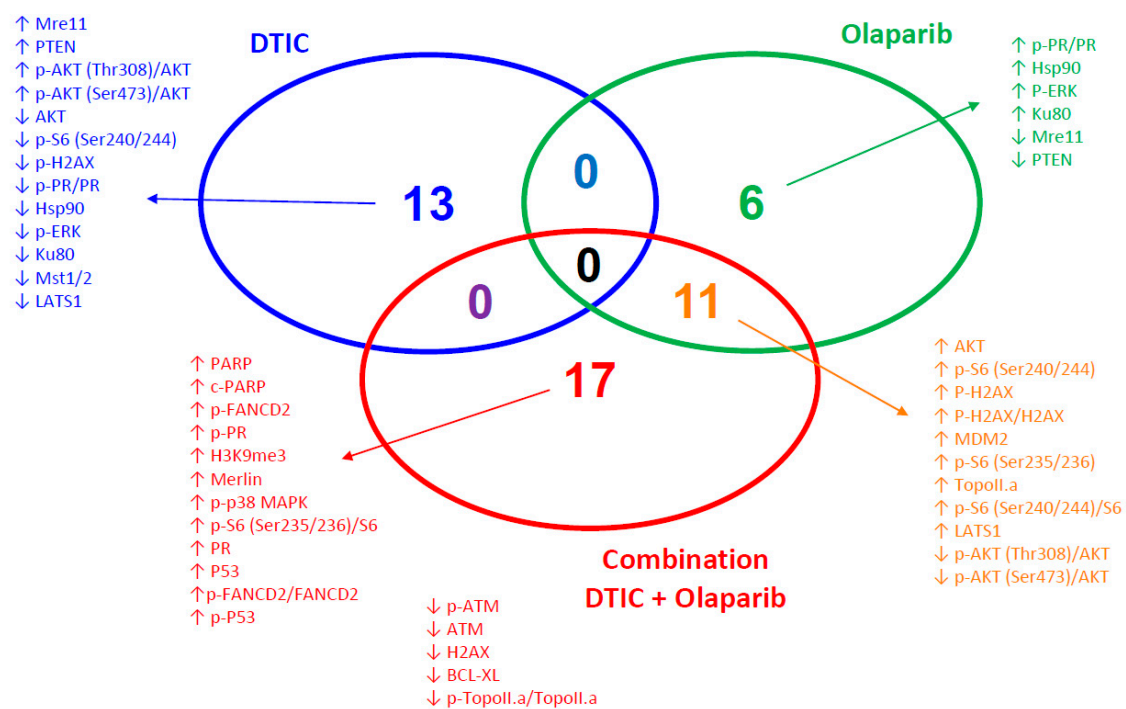


Figure 4. Venn diagram of the proteins significantly ($p < 0.01$) correlated to response to DTIC alone (blue) (MP55 + MP77 + MM52 versus MM33), olaparib alone (green) (MM33 versus MP55 + MP77 + MM52), or the DTIC + olaparib combination (red) (MP55 + MP77 + MM33 versus MM52) (paired t tests assuming equal variance).

We evaluated protein expression modifications under the different therapies by comparing untreated mice with treated mice for each PDX model. We observed modifications in DNA repair proteins, both in homologous recombination (HR) and nonhomologous end joining (NHEJ) pathways (Table S3), as illustrated in Figure 5 for one model showing a synergy between DTIC and olaparib (MP55) and one model showing no synergy (MM52). We did not identify modifications that could be correlated to the additive effect of DTIC + olaparib compared to DTIC alone.

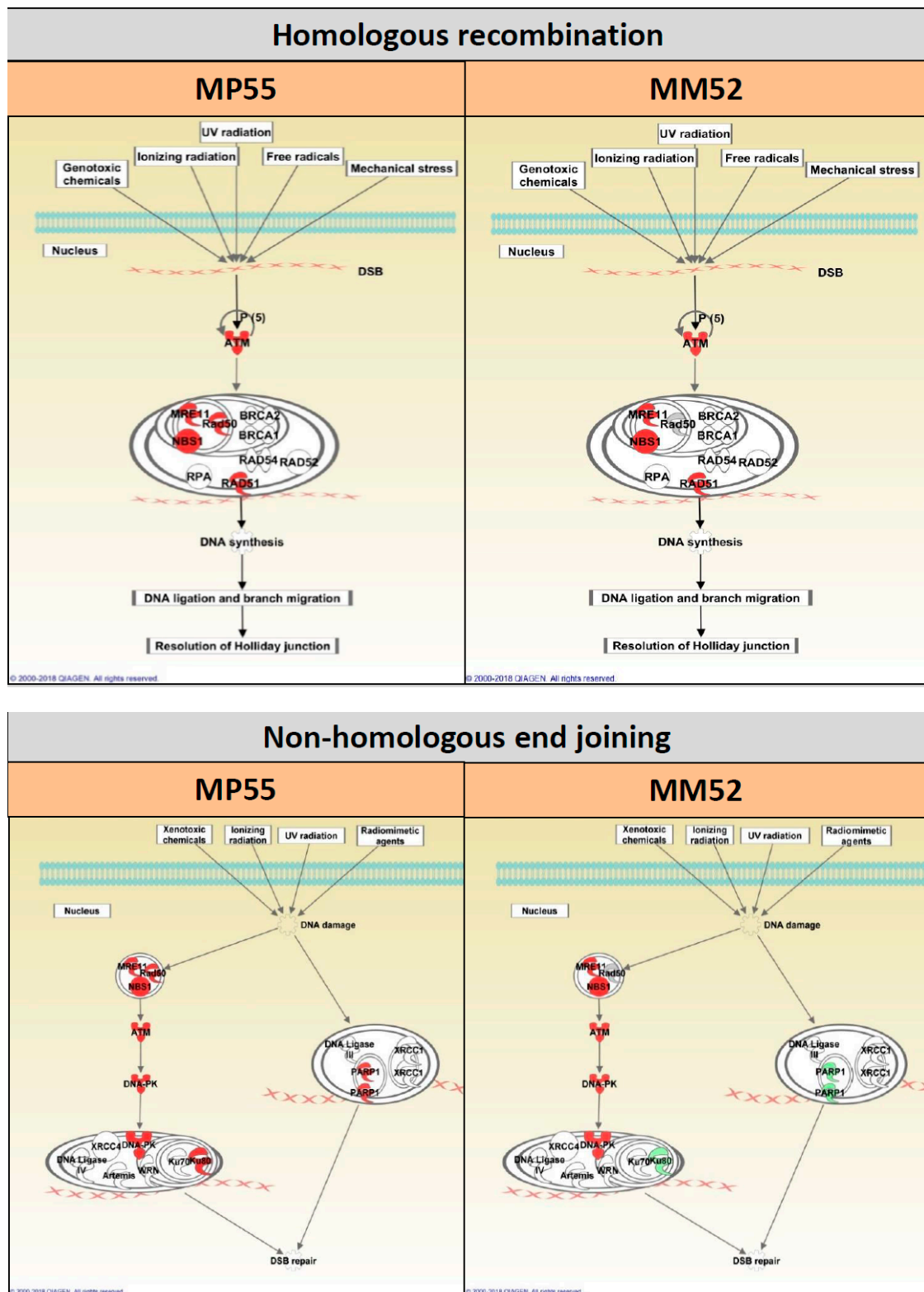


Figure 5. Schematic representation of HR- and NHEJ-related protein expression modifications in the two PDXs MP55 and MM52: Olaparib + DTIC versus DTIC. The intensity of color reflects fold change. Red color: higher (phospho-)protein expression in olaparib + DTIC than in DTIC alone. Green color: lower (phospho-)protein expression in olaparib + DTIC than in DTIC alone.

When looking at apoptosis induction studied by PARP and cleaved-PARP expressions, we did not observe significant variations between tumors collected after DTIC or DTIC + olaparib treatments, except in the MM33 PDX (Figure S11 and Table S4). Moreover, we did not observe significant variations of cleaved-PARP expression after DTIC administration, except in the MM52 PDX. Finally, the study of RPPA-based apoptosis-related protein expression (Bcl-2, Bcl-X_L, Mcl1, Bax, and Bak) showed that both anti- and proapoptotic protein expressions were modified after DTIC + olaparib administration, in comparison to the control group (Figure S12 and Table S5). These data were confirmed by Western Blot (Figures S13–S17; Table S6) and IHC (Figure S18) and suggest that apoptosis may not be implicated in the additive effect observed after DTIC + olaparib treatment.

In addition, both MAPK and Pi3K signaling pathways were studied by RPPA, showing no significant recurrent protein expression variations between DTIC- and DTIC + olaparib-treated tumors (Figures S19 and S20; Tables S7 and S8). This was confirmed by western blot (Figures S21 and S22) and IHC (Figures S23 and S24).

Finally, we have also studied Hippo-related protein modifications in the four selected PDXs (Figure S25 and Table S9). We observed a highly significant increase of p-YAP (phospho-Yes-associated protein) expression in most mice upon DTIC treatment (Figure S26). These observations were confirmed by IHC, where we observed a high and significant increase of both nuclear and/or cytoplasm YAP and TAZ expression under olaparib alone, DTIC alone, and olaparib + DTIC in all but one (MM33) PDXs (Figure 6 and Figure S27). This result suggests that DTIC does not only induce DNA damage but might also exert an antitumor effect through YAP phosphorylation.

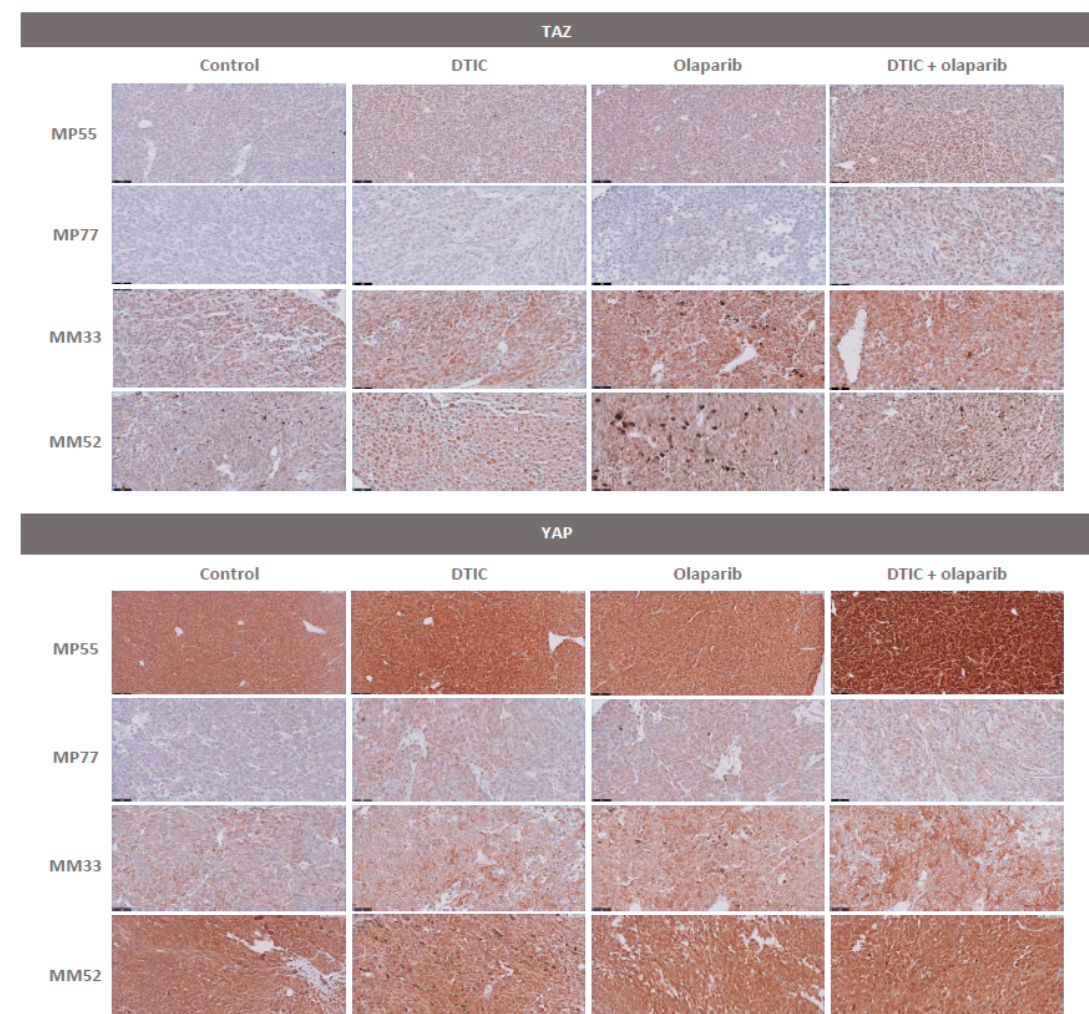


Figure 6. TAZ and YAP protein staining in the four treated PDXs by IHC.

3. Discussion

In this work, we aimed to evaluate the therapeutic potential of the PARP inhibitor olaparib in UM PDXs for the first time. Because PARP expression or activity is potentially predictive for response to PARP inhibition [31], we first confirmed that the PARP gene family is expressed and activated at similar levels in our panel of 11 well-characterized PDX models compared to corresponding patient samples. This is the case at least for the PARP 1–4 genes, which are targeted by olaparib [32]. Next, we showed that olaparib alone was not efficient, but significantly increased the response to the alkylating agent dacarbazine. In contrast, such an additive effect was not observed when olaparib was combined with other compounds, i.e., the alkylating agent fotemustine, the mTORC1 inhibitor everolimus, the PKC inhibitor AEB071, the MDM2 inhibitor CGM097, the ATM inhibitor AZD0156, and the ATR inhibitor AZD6738.

An additive activity of PARP inhibitor combined with chemotherapeutic agents has already been reported, even in the absence of BRCA1/2 mutation, for the isoquinoline alkylating agent trabectedin [33], camptothecins [34], and, of course, temozolomide/dacarbazine [34–36]. The increased *in vivo* activity of dacarbazine in UM PDXs when combined with olaparib could be explained by the fact that PARP inhibition increases the antitumor effects of DNA-damaging through disruption of the base excision repair pathway function, as previously reported [37]. In addition, BAP1 deficiency might confer a moderate DNA repair deficiency, in a similar manner as BRCA1 deficient tumors, and thus confer an increased sensitivity to olaparib upon DNA damage induction by DTIC. However, among our three models that show an additive effect between olaparib and DTIC, only one (MP55) had a detectable BAP1 mutation (Table S10). Although the number of models is too low to draw conclusions, olaparib might affect tumor growth independently of BAP1 status, as has been observed in malignant pleural mesothelioma [38]. Alternatively, BAP1 deficiency may not only be induced by mutations. Several studies have indeed reported the absence of nuclear BAP1 protein despite the presence of a wild-type gene [39–42] and normal mRNA levels [43], suggesting that post-translational regulation, for example by miR31 [44,45], can also induce functional BAP1 deficiency. However, this type of regulation does not seem to be at play in our models, since BAP1 mutation status and IHC staining are concordant. Surprisingly, we did not observe a similar synergy between olaparib and fotemustine. This may be explained by a slightly different mode of action between the two compounds, or by the fact that fotemustine + olaparib was tested in only two PDXs (Figure S2) and statistical power may thus be insufficient to detect an additive effect.

We also aimed to identify biomarkers of prediction for an additive efficiency of dacarbazine combined with olaparib. While response to DTIC alone seems to be associated with decreased activation of PI3K/Akt and MEK/ERK signaling and decreased expression of components of the Hippo pathway (MST1/2 and LATS), we have identified two classes of proteins predictive for the combination of dacarbazine with olaparib: those involved in DNA repair (high expression of PARP, c-PARP, p-FANCD2, p-FANCD2/FANCD2, P53, and p-P53, and low expression of ATM, p-ATM, and p-Topo.IIa/Topo.IIa), and those involved in apoptosis (low Bcl-X_L protein). High PARP expression has already been identified as being predictive for the synergy between olaparib and the alkylating agent trabectedin [33]. More generally, several proteins involved in DNA damage repair are known as predictive biomarkers for PARP inhibition [46,47]. We also showed that a low expression of the antiapoptotic Bcl-X_L protein was a highly predictive marker for the additive efficacy of dacarbazine + olaparib ($p = 5.1 \times 10^{-4}$). Our observation is concordant with that of Engert and colleagues, showing that olaparib + temozolomide combination induced downregulation of the antiapoptotic protein MCL-1, and the activation of the two proapoptotic proteins BAX and BAK with apoptosis occurrence (mitochondrial outer membrane permeabilization and caspase-3 activation) [35], altogether suggesting the possible role of apoptosis-regulatory proteins as predictive markers of response or proteins that are impacted by such treatments. This observation suggests that a Bcl-X_L inhibitor may be useful to sensitize tumors to the concomitant administration of dacarbazine + olaparib.

Finally, we have also made a very striking observation in the view of UM. It was previously reported that *GNAQ/GNA11* mutations induce dephosphorylation and thus nuclear accumulation of the YAP protein [19,48], both through a Hippo-independent and a Hippo-dependent pathway [8,9]. Verteporfin, known to disrupt the interaction between YAP and TEAD4, was indeed able to induce apoptosis of UM cells [49]. In our study, we observed a strong and significant increase of both YAP and TAZ protein expression and phosphorylation upon treatment with DTIC and, to a lesser extent, olaparib. Those results therefore suggest that these drugs may exert their antitumor effect also through phosphorylation and thus inactivation of YAP. Administration of verteporfin in addition to DTIC + olaparib might be a path to explore in order to further potentiate the synergy of the combination treatment.

4. Materials and Methods

4.1. Uveal Melanoma Preclinical Models

Eleven PDXs representative of the UM disease were used, five obtained from primary intraocular tumors (MP34, MP41, MP42, MP55, and MP77), five from liver metastatic tumor samples (MM26, MM52, MM66, MM224, and MM252), and one from cutaneous metastasis (MM33). Molecular features of these models are presented in the Table S10. Some of these PDXs have already been reported [28,29].

4.2. Compounds

The PARP inhibitor olaparib, partially provided from Novartis Institutes for Biomedical Research (NIBR, Cambridge, UK) and Astra-Zeneca (Oncology Bioscience, Cambridge, UK), was orally administered at a daily dose of 50 mg/kg or 100 mg/kg, five days a week, depending to the tolerance of tested combinations. Two cytotoxic agents were tested, both alkylating agents, i.e., dacarbazine (Deticene[®] or DTIC) (Medac, Lyon, France) and fotemustine (Muphoran[®]) (IRIS, Orly, France). Five different targeted therapies were used, the mTORC1 inhibitor everolimus (RAD001, Certican[®]) (Novartis, Basel, Switzerland), the pan-PKC inhibitor AEB071 (provided from Novartis), the MDM2 inhibitor CGM097 (provided from Novartis), the ATM inhibitor AZD0156 (provided from Astra-Zeneca), and the ATR inhibitor AZD6738 (provided from Astra-Zeneca). All treatment schedules are presented in the Table S11.

4.3. In vivo Tumor Growth and Antitumor Efficacy

For in vivo therapeutic studies, female SCID mice (Janvier Labs, Le Genest Saint Isle, France) were xenografted with a tumor fragment of 20–40 mm³. Mice bearing growing tumors with a volume of 60–150 mm³ were randomly assigned to the control or treatment groups. The number of animals per group was related to the date of experiments. While initial in vivo experiments were performed with about seven to ten mice per group, final experiments, for ethical reasons and to decrease the cost of the study, were performed according to a related- “single-mouse” schedule in which three mice bearing growing tumor were included per group [11,50]. Overall, due to the fact that this study was conducted during a relatively long period, about two years of in vivo experiments, the number of models used for each combination of treatments and the number of mice per model was not homogeneous along the study. Treatments were started on day one. Mice were weighed and tumors measured twice a week. Xenografted mice were sacrificed when their tumor reached a volume of 2500 mm³.

Mice bearing tumors with a volume from 50 to 150 mm³ were individually identified and randomly assigned to the control or treatment groups. Tumor growth was evaluated by measurement twice a week of two perpendicular diameters of tumors with a caliper. Individual tumor volume, relative tumor volume (RTV), and tumor growth inhibition (TGI) were calculated according to standard methodology [51]. Moreover, to evaluate the overall response rate (ORR) to treatments observed in all treated models according to individual mouse variability, we decided to consider each mouse as one tumor-bearing entity. Hence, in all in vivo experiments, a relative tumor volume variation (RTVV)

of each treated mouse was calculated from the following formula: $[(RTV_t/mRTV_c)]$, where RTV_t is the relative tumor volume of the treated mouse and $mRTV_c$ the median relative tumor volume of the corresponding control group at a time corresponding to the end of treatment. Then, for each treated mouse, we calculated $[(RTV)-1]$. Finally, to clearly evaluate the impact of treatments on the tumor progression, we evaluated the probability of progression (doubling time and time for $RTV \times 4$).

In each *in vivo* experiment, frozen and formol-fixed tumor tissues were collected at the time of first ethical sacrifice in all treated groups, which depends on the tumor growth speed of each PDX. Between three to five tumors have been obtained from each group, according to the experimental design.

Statistical significance of observed differences between the individual RTVs corresponding to the treated mice and control groups was calculated using the two tailed Mann–Whitney test. Statistical significance of ORR between tested treatments was determined using a χ^2 test. Predictive markers have been defined using a Mann–Whitney test.

Studies have been performed in compliance with the recommendations of the French Ethical Committee and under the supervision of authorized investigators. The experimental protocol and animal housing followed institutional guidelines as put forth by the French Ethical Committee (Agreement number D-750602, France) and the ethics committee of the Institut Curie (Agreement number C75-05-18).

4.4. Microarray Analysis—Transcriptome Arrays

mRNA gene expression of patient tumors and corresponding xenografts was defined using Human Exon 1.0 ST Array (Affymetrix, Santa Clara, CA, USA). RNA extraction, array hybridization, and analyses were performed as previously reported [29].

4.5. Reverse Phase Protein Array Study (RPPA)

RPPA methodology and analysis were performed as previously described [29]. Two different studies were performed: (i) A first one on 15 UM PDXs and their originating patient's tumors identified in Némati et al. [17]; in this cohort, RPPA-based protein expressions were studied in the original patient tumors and corresponding xenografts at very early (P1), early (P4), and late (P9) *in vivo* passages in SCID mice. (ii) A second one on four to six tumors per group obtained at the end of four *in vivo* experiments evaluating the olaparib + DTIC combination (MP55, MP77, MM33, and MM52 PDXs). Differential abundance of the proteins between various tumor cohorts and groups was assessed using paired *t* tests assuming equal variance. The list of studied proteins and of used primary antibodies is presented in the Table S12.

4.6. Western Blot (WB) Analyses

Proteins were extracted as described previously [52]. Lysates were resolved on 4–12% TGX gels (Bio-Rad[®], manufacturer, Marnes La Coquette, France). RNA extraction, array hybridization, and analyses were performed as previously reported [29].), transferred to nitrocellulose membranes (Bio-Rad[®]). Immunoblotting was performed with antibodies against the ubiquitous protein GAPDH and some other specific studied proteins, as shown in the Table S13. After washes, membranes were incubated with the appropriate secondary horseradish peroxidase-conjugated affinity-purified goat anti-rabbit antibody (Jackson Immuno Research Laboratories, Inc., Interchim, San Diego, CA, USA). Quantification of protein expression was performed using Multi Gauge software and normalized to GAPDH expression. For each PDX model, the ratio of p-protein/protein in treated tumors was calculated.

4.7. Immunohistochemical (IHC) Study

Immunohistochemical analyses were performed for the following pathways: Apoptosis and cell proliferation (caspase 3, cleaved-caspase 3, PARP, cleaved PARP, p-H2AX, and Ki67), the MAPK pathway (MEK1/2, p-MEK1/2, ERK, and p-ERK), the Pi3K pathway (AKT, p-AKT, S6, and p-S6), and the Hippo-related pathway (YAP and TAZ proteins). The list of all used antibodies is presented in the Table S14. Paraffin-embedded tissue blocks and TMAs were cut with a microtome into fine slivers of 3 microns. Tissue sections were dewaxed and rehydrated through a series of xylene and ethanol washes before heat-induced epitope retrieval. Immunostaining was processed by using a Dako automated. The slides were incubated with primary antibody one hour at room temperature or overnight at 4 °C and then with secondary antibody coupled to horseradish peroxidase. For two antibodies (p-H2AX and cleaved-caspase3), the secondary antibody was biotinylated and the section incubated with ABC system. A DAB solution was applied for five minutes to reveal peroxidase. Slides were counterstained with hematoxylin before mounting with resin. A pathological score (0 to 3) was defined as % of positive cells (0 to 1) × intensity of immunostaining (0 to 3).

5. Conclusions

In conclusion, our work demonstrates that olaparib might be helpful in the treatment of metastatic UM patients when combined with dacarbazine. Such a combination should be tested after assessment of various predictive markers that we have also identified, and may be, if clinical tolerance is acceptable, associated with a Bcl-X_L inhibitor or a YAP inhibitor.

Supplementary Materials: The following are available online at <http://www.mdpi.com/2072-6694/11/6/751/s1>; Figure S1: Affymetrix-based PARP family gene expression, Figure S2: Affymetrix-based PARP family gene expression, Figure S3: Combination of olaparib and fotemustine, Figure S4: Combination of olaparib and everolimus, Figure S5: Combination of olaparib and AEB071, Figure S6: Combination of olaparib and CGM097, Figure S7: Combination of olaparib and AZD0156, Figure S8: Combination of olaparib and AZD6738, Figure S9: Significant protein expression between PDXs with additive efficacy (MP55-MP77-MM33) and PDX without additive efficacy (MM52) of the DTIC + olaparib combination ($p < 0.05$), Figure S10: Significant protein expression between PDXs with additive efficacy (MP55-MP77-MM33) and PDX without additive efficacy (MM52) of the DTIC + olaparib combination, Figure S11: RPPA-based PARP and c-PARP protein expression, Figure S12: RPPA-based Apoptosis-related protein expression, Figure S13: MP55 PDX, Figure S14: MP77 PDX, Figure S15: MM33 PDX, Figure S16: MM52 PDX, Figure S17: WB-based PARP and c-PARP protein expression, Figure S18: IHC-based apoptosis-and cell proliferation-related protein expression, Figure S19: RPPA-based MAPK-related protein expression, Figure S20: RPPA-based Pi3K-related protein expression, Figure S21: WB-based MAPK-related protein expression, Figure S22: WB-based Pi3K-related protein expression, Figure S23: IHC-based MAPK-related protein expression, Figure S24: IHC-based Pi3K-related protein expression, Figure S25: RPPA-based Hippo-related protein expression, Figure S26: Hippo-related expression modifications in four treated PDXs, Figure S27: IHC-based Hippo-related protein expression, Table S1: p values and Fold Changes (FC) in all pair comparisons of RPPA-based PARP protein expression, Table S2: Treatments received by the UM PDX panel, Table S3: Comparisons of RPPA-based DNA repair-related protein expression between in vivo experimental groups, Table S4: Comparisons of RPPA-based PARP protein expression between in vivo experimental groups, Table S5: Comparisons of RPPA-based Apoptose-related protein expression between in vivo experimental groups, Table S6: Comparisons of WB-based protein expression between in vivo experimental groups, Table S7: Comparisons of RPPA-based MAPK-related protein expression between in vivo experimental groups, Table S8: Comparisons of RPPA-based Pi3K-related protein expression between in vivo experimental groups, Table S9: Comparisons of RPPA-based Hippo-related protein expression between in vivo experimental groups, Table S10: Main characteristics of the used uveal melanoma PDXs, Table S11: Compounds tested in in vivo experiments, Table S12: List of the proteins studied by RPPA between patient's tumors and corresponding PDXs, Table S13: List of the proteins studied by Western Blots and their corresponding used antibodies, Table S14: List of the proteins studied by IHC and their corresponding used antibodies.

Author Contributions: L.d.K. analysed RPPA data, analysed all data, helped writing the manuscript. D.D. designed experiments, analysed all data, helped writing the manuscript. R.E.B. performed WB. A.N. (André Nicolas) performed IHC experiments. G.C., M.S., A.N. (Adnan Naguez) and J.F. performed in vivo studies. B.O. and A.C. performed RPPA experiments. V.C., A.W., P.S. and E.M. helped writing the manuscript. D.G. performed and analysed Affymetrix analyses. D.M. analysed IHC data. P.M., N.C., S.P.-N. and S.P.-R. provided patient material for PDX development, clinical insight and critical feedback. F.N. helped writing the manuscript.

Funding: The project was supported by a grant from the Fondation de France.

Acknowledgments: We wish to thank the Animal Platform CRP2-UMS 3612 CNRS-US25 Inserm-IRD (Faculty of Pharmacy, Paris Descartes University, Paris), and the animal Platform of the Institut Curie. The study was partially supported by “La Fondation de France”, and by Novartis and Astra-Zeneca laboratories, who are included in the authors. Novartis and Astra-Zeneca laboratories provided the molecules (Novartis provided AEB071, olaparib and CGM097. Astra-Zeneca provided AZD0156, AZD6738 and olaparib), and Novartis financed a part of the experiments.

Conflicts of Interest: We declare the following conflicts of interest: the study was supported by Novartis and Astra-Zeneca laboratories, who are included in the authors. They provided the molecules (Novartis provided AEB071, olaparib and CGM097. Astra-Zeneca provided AZD0156, AZD6738 and olaparib), Novartis financed a part of the experiments, and both reviewed the manuscript.

References

1. Singh, A.D.; Bergman, L.; Seregard, S. Uveal melanoma: Epidemiologic aspects. *Ophthalmol. Clin. N. Am.* **2005**, *18*, 75–84. [[CrossRef](#)] [[PubMed](#)]
2. Amaro, A.; Gangemi, R.; Piaggio, F.; Angelini, G.; Barisione, G.; Ferrini, S.; Pfeffer, U. The biology of uveal melanoma. *Cancer Metastasis Rev.* **2017**, *36*, 109–140. [[CrossRef](#)] [[PubMed](#)]
3. Reichstein, D. New concepts in the molecular understanding of uveal melanoma. *Curr. Opin. Ophthalmol.* **2017**, *28*, 219–227. [[CrossRef](#)] [[PubMed](#)]
4. Sato, T.; Han, F.; Yamamoto, A. The biology and management of uveal melanoma. *Curr. Oncol. Rep.* **2008**, *10*, 431–438. [[CrossRef](#)] [[PubMed](#)]
5. Abildgaard, S.K.; Vorum, H. Proteomics of uveal melanoma: A mini review. *J. Oncol.* **2013**, *2013*, 820953. [[CrossRef](#)] [[PubMed](#)]
6. Nichols, E.E.; Richmond, A.; Daniels, A.B. Tumor characteristics, genetics, management, and the risk of metastasis in uveal melanoma. *Semin. Ophthalmol.* **2016**, *31*, 304–309. [[CrossRef](#)] [[PubMed](#)]
7. Sharma, D.A.; Stei, M.M.; Fröhlich, H.; Holz, F.G.; Loeffler, K.U. Genetic and epigenetic insights into uveal melanoma. *Clin. Genet.* **2018**, *94*, 308. [[CrossRef](#)]
8. Feng, X.; Degese, M.S.; Iglesias-Bartolome, R.; Vaque, J.P.; Molinolo, A.A.; Rodrigues, M.; Zaidi, M.R.; Ksander, B.R.; Merlino, G.; Sodhi, A.; et al. Hippo-independent activation of YAP by the GNAQ uveal melanoma oncogene through a trio-regulated rho GTPase signaling circuitry. *Cancer Cell* **2014**, *25*, 831–845. [[CrossRef](#)]
9. Feng, X.; Arang, N.; Rigeracciolo, D.C.; Lee, J.S.; Yeerna, H.; Wang, Z.; Lubrano, S.; Kishore, A.; Pachter, J.A.; König, G.M.; et al. A Platform of Synthetic Lethal Gene Interaction Networks Reveals that the GNAQ Uveal Melanoma Oncogene Controls the Hippo Pathway through FAK. *Cancer Cell* **2019**, *35*, 457–472. [[CrossRef](#)]
10. Carvajal, R.D.; Piperno-Neumann, S.; Kapiteijn, E.; Kapiteijn, E.; Chapman, P.B.; Frank, S.; Joshua, A.M.; Piulats, J.M.; Wolter, P.; Cocquyt, V.; et al. Selumetinib in combination with dacarbazine in patients with metastatic uveal melanoma: A Phase III, multicenter, randomized trial (SUMIT). *J. Clin. Oncol.* **2018**, *36*, 1232–1239. [[CrossRef](#)]
11. Decaudin, D.; El Botty, R.; Diallo, B.; Massonnet, G.; Fleury, J.; Naguez, A.; Raymondie, C.; Davies, E.; Smith, A.; Wilson, J.; et al. Selumetinib-based therapy in uveal melanoma patient-derived xenografts. *Oncotarget* **2018**, *9*, 21674–21686. [[CrossRef](#)] [[PubMed](#)]
12. Carita, G.; Frisch-Dit-Leitz, E.; Dahmani, A.; Raymondie, C.; Cassoux, N.; Piperno-Neumann, S.; Némati, F.; Laurent, C.; De Koning, L.; Halilovic, E.; et al. Dual inhibition of protein kinase C and p53-MDM2 or PKC and mTORC1 are novel efficient therapeutic approaches for uveal melanoma. *Oncotarget* **2016**, *7*, 33542–33556. [[CrossRef](#)] [[PubMed](#)]
13. Harbour, J.W.; Onken, M.D.; Roberson, E.D.; Duan, S.; Cao, L.; Worley, L.A.; Council, M.L.; Matatall, K.A.; Helms, C.; Bowcock, A.M. Frequent mutation of BAP1 in metastasizing uveal melanomas. *Science* **2010**, *330*, 1410–1413. [[CrossRef](#)] [[PubMed](#)]
14. Kujala, E.; Mäkitie, T.; Kivelä, T. Very long-term prognosis of patients with malignant uveal melanoma. *Investig. Ophthalmol. Vis. Sci.* **2003**, *44*, 4651–4659. [[CrossRef](#)] [[PubMed](#)]
15. Augsburger, J.J.; Corrêa, Z.M.; Shaikh, A.H. Effectiveness of treatments for metastatic uveal melanoma. *Am. J. Ophthalmol.* **2009**, *148*, 119–127. [[CrossRef](#)] [[PubMed](#)]
16. Masoomian, B.; Shields, J.A.; Shields, C.L. Overview of BAP1 cancer predisposition syndrome and the relationship to uveal melanoma. *J. Curr. Ophthalmol.* **2018**, *30*, 102–109. [[CrossRef](#)] [[PubMed](#)]

17. Fukuda, T.; Tsuruga, T.; Kuroda, T.; Nishikawa, H.; Ohta, T. Functional Link between BRCA1 and BAP1 through Histone H2A, Heterochromatin and DNA Damage Response. *Curr. Cancer Drug Targets* **2016**, *16*, 101–109. [[CrossRef](#)] [[PubMed](#)]
18. Ismail, I.H.; Davidson, R.; Gagné, J.P.; Xu, Z.Z.; Poirier, G.G.; Hendzel, M.J. Germline mutations in BAP1 impair its function in DNA double-strand break repair. *Cancer Res.* **2014**, *74*, 4282–4294. [[CrossRef](#)] [[PubMed](#)]
19. Yu, H.; Pak, H.; Hammond-Martel, I.; Ghram, M.; Rodrigue, A.; Daou, S.; Barbour, H.; Corbeil, L.; Hébert, J.; Drobetsky, E.; et al. Tumor suppressor and deubiquitinase BAP1 promotes DNA double-strand break repair. *Proc. Natl. Acad. Sci. USA* **2014**, *111*, 285–290. [[CrossRef](#)]
20. Liu, X.; Kumar, M.; Yang, L.; Molkentine, D.P.; Valdecanas, D.; Yu, S.; Meyn, R.E.; Heymach, J.V.; Skinner, H.D. BAP1 Is a Novel Target in HPV-Negative Head and Neck Cancer. *Clin. Cancer Res.* **2018**, *24*, 600–607. [[CrossRef](#)]
21. Helleday, T.; Petermann, E.; Lundin, C.; Hodgson, B.; Sharma, R.A. DNA repair pathways as targets for cancer therapy. *Nat. Rev. Cancer* **2008**, *8*, 193–204. [[CrossRef](#)] [[PubMed](#)]
22. McCabe, N.; Turner, N.C.; Lord, C.J.; Kluzek, K.; Bialkowska, A.; Swift, S.; Giavara, S.; O'Connor, M.J.; Tutt, A.N.; Zdzienicka, M.Z.; et al. Deficiency in the repair of DNA damage by homologous recombination and sensitivity to poly(ADP-ribose) polymerase inhibition. *Cancer Res.* **2006**, *66*, 8109–8115. [[CrossRef](#)] [[PubMed](#)]
23. Molloy-Simard, V.; St-Laurent, J.F.; Vigneault, F.; Gaudreault, M.; Dargis, N.; Guérin, M.C.; Leclerc, S.; Morcos, M.; Black, D.; Molgat, Y.; et al. Altered expression of the poly(ADP-ribosyl)ation enzymes in uveal melanoma and regulation of PARG gene expression by the transcription factor ERM. *Investig. Ophthalmol. Vis. Sci.* **2012**, *53*, 6219–6231. [[CrossRef](#)] [[PubMed](#)]
24. Géhl, Z.; Bai, P.; Bodnár, E.; Emri, G.; Remenyik, É.; Németh, J.; Gergely, P.; Virág, L.; Szabó, É. Poly(ADP-ribose) in the skin and in melanomas. *Histol. Histopathol.* **2012**, *27*, 651–659. [[PubMed](#)]
25. Némati, F.; de Montrion, C.; Lang, G.; Kraus-Berthier, L.; Carita, G.; Sastre-Garau, X.; Berniard, A.; Vallerand, D.; Geneste, O.; de Plater, L.; et al. Targeting Bcl-2/Bcl-XL induces antitumor activity in uveal melanoma patient-derived xenografts. *PLoS ONE* **2014**, *9*, e80836. [[CrossRef](#)] [[PubMed](#)]
26. Amirouchene-Angelozzi, N.; Frisch-Dit-Leitz, E.; Carita, G.; Dahmani, A.; Raymondie, C.; Liot, G.; Gentien, D.; Némati, F.; Decaudin, D.; Roman-Roman, S.; et al. The mTOR inhibitor Everolimus synergizes with the PI3K inhibitor GDC0941 to enhance antitumor efficacy in uveal melanoma. *Oncotarget* **2016**, *7*, 23633–23646. [[CrossRef](#)] [[PubMed](#)]
27. Piperno-Neumann, S.; Diallo, A.; Etienne-Grimaldi, M.C.; Bidard, F.C.; Rodrigues, M.; Plancher, C.; Mariani, P.; Cassoux, N.; Decaudin, D.; Asselain, B.; et al. Phase II Trial of Bevacizumab in Combination with Temozolomide as First-Line Treatment in Patients with Metastatic Uveal Melanoma. *Oncologist* **2016**, *21*, 281–282. [[CrossRef](#)] [[PubMed](#)]
28. Némati, F.; Sastre-Garau, X.; Laurent, C.; Couturier, J.; Mariani, P.; Desjardins, L.; Piperno-Neumann, S.; Lantz, O.; Asselain, B.; Plancher, C.; et al. Establishment and Characterization of a Panel of Human Uveal Melanoma Xenografts Derived from Primary and/or Metastatic Tumors. *Clin. Cancer Res.* **2010**, *16*, 2352–2362. [[CrossRef](#)] [[PubMed](#)]
29. Laurent, C.; Gentien, D.; Piperno-Neumann, S.; Némati, F.; Nicolas, A.; Tesson, B.; Desjardins, L.; Mariani, P.; Rapinat, A.; Sastre-Garau, X.; et al. Patient-derived xenografts recapitulate molecular features of human uveal melanomas. *Mol. Oncol.* **2013**, *7*, 625–636. [[CrossRef](#)] [[PubMed](#)]
30. Del Rivero, J.; Kohn, E.C. PARP Inhibitors: The Cornerstone of DNA Repair-Targeted Therapies. *Oncology* **2017**, *31*, 265–273. [[PubMed](#)]
31. Bitler, B.G.; Watson, Z.L.; Wheeler, L.J.; Behbakht, K. PARP inhibitors: Clinical utility and possibilities of overcoming resistance. *Gynecol. Oncol.* **2017**, *147*, 695–704. [[CrossRef](#)] [[PubMed](#)]
32. Wahlberg, E.; Karlberg, T.; Kouznetsova, E.; Markova, N.; Macchiarulo, A.; Thorsell, A.G.; Pol, E.; Frostell, Å.; Ekblad, T.; Öncü, D.; et al. Family-wide chemical profiling and structural analysis of PARP and tankyrase inhibitors. *Nat. Biotechnol.* **2012**, *30*, 283–288. [[CrossRef](#)] [[PubMed](#)]
33. Pignochino, Y.; Capozzi, F.; D'Ambrosio, L.; Dell'Aglio, C.; Basiricò, M.; Canta, M.; Lorenzato, A.; Vignolo, L.F.; Aliberti, S.; Palesandro, E.; et al. PARP1 expression drives the synergistic antitumor activity of trabectedin and PARP1 inhibitors in sarcoma preclinical models. *Mol. Cancer* **2017**, *16*, 86. [[CrossRef](#)] [[PubMed](#)]

34. Murai, J.; Zhang, Y.; Morris, J.; Ji, J.; Takeda, S.; Doroshow, J.H.; Pommier, Y. Rationale for poly(ADP-ribose) polymerase (PARP) inhibitors in combination therapy with camptothecins or temozolomide based on PARP trapping versus catalytic inhibition. *J. Pharmacol. Exp. Ther.* **2014**, *349*, 408–416. [[CrossRef](#)] [[PubMed](#)]
35. Engert, F.; Schneider, C.; Weiß, L.M.; Probst, M.; Fulda, S. PARP Inhibitors Sensitize Ewing Sarcoma Cells to Temozolomide-Induced Apoptosis via the Mitochondrial Pathway. *Mol. Cancer Ther.* **2015**, *14*, 2818–2830. [[CrossRef](#)] [[PubMed](#)]
36. Lok, B.H.; Gardner, E.E.; Schneeberger, V.E.; Ni, A.; Desmeules, P.; Rekhman, N.; de Stanchina, E.; Teicher, B.A.; Riaz, N.; Powell, S.N.; et al. PARP Inhibitor Activity Correlates with SLFN11 Expression and Demonstrates Synergy with Temozolomide in Small Cell Lung Cancer. *Clin. Cancer Res.* **2017**, *23*, 523–535. [[CrossRef](#)] [[PubMed](#)]
37. Khan, O.A.; Gore, M.; Lorigan, P.; Stone, J.; Greystoke, A.; Burke, W.; Carmichael, J.; Watson, A.J.; McGown, G.; Thorncroft, M.; et al. A phase I study of the safety and tolerability of olaparib (AZD2281, KU0059436) and dacarbazine in patients with advanced solid tumours. *Br. J. Cancer* **2011**, *104*, 750–755. [[CrossRef](#)] [[PubMed](#)]
38. Srinivasan, G.; Sidhu, G.S.; Williamson, E.A.; Jaiswal, A.S.; Najmunnisa, N.; Wilcoxon, K.; Jones, D.; George, T.J., Jr.; Hromas, R. Synthetic lethality in malignant pleural mesothelioma with PARP1 inhibition. *Cancer Chemother. Pharmacol.* **2017**, *80*, 861–867. [[CrossRef](#)] [[PubMed](#)]
39. Righi, L.; Duregon, E.; Vatrano, S.; Izzo, S.; Giorelli, J.; Rondón-Lagos, M.; Ascoli, V.; Ruffini, E.; Ventura, L.; Volante, M.; et al. BRCA1-Associated Protein 1 (BAP1) Immunohistochemical Expression as a Diagnostic Tool in Malignant Pleural Mesothelioma Classification: A Large Retrospective Study. *J. Thorac. Oncol.* **2016**, *11*, 2006–2017. [[CrossRef](#)] [[PubMed](#)]
40. Farquhar, N.; Thornton, S.; Coupland, S.E.; Coulson, J.M.; Sacco, J.J.; Krishna, Y.; Heimann, H.; Taktak, A.; Cebulla, C.M.; Abdel-Rahman, M.H.; et al. Patterns of BAP1 protein expression provide insights into prognostic significance and the biology of uveal melanoma. *J. Pathol. Clin. Res.* **2017**, *4*, 26–38. [[CrossRef](#)] [[PubMed](#)]
41. Koopmans, A.E.; Verdijk, R.M.; Brouwer, R.W.; van den Bosch, T.P.; van den Berg, M.M.; Vaarwater, J.; Kockx, C.E.; Paridaens, D.; Naus, N.C.; Nellist, M.; et al. Clinical significance of immunohistochemistry for detection of BAP1 mutations in uveal melanoma. *Mod. Pathol.* **2014**, *27*, 1321–1330. [[CrossRef](#)] [[PubMed](#)]
42. Yavuziyigitoglu, S.; Drabarek, W.; Smit, K.N.; van Poppel, N.; Koopmans, A.E.; Vaarwater, J.; Brands, T.; Eussen, B.; Dubbink, H.J.; van Riet, J.; et al. Rotterdam Ocular Melanoma Study Group. Correlation of Gene Mutation Status with Copy Number Profile in Uveal Melanoma. *Ophthalmology* **2017**, *124*, 573–575. [[CrossRef](#)]
43. Bott, M.; Brevet, M.; Taylor, B.S.; Shimizu, S.; Ito, T.; Wang, L.; Creaney, J.; Lake, R.A.; Zakowski, M.F.; Reva, B.; et al. The nuclear deubiquitinase BAP1 is commonly inactivated by somatic mutations and 3p21.1 losses in malignant pleural mesothelioma. *Nat. Genet.* **2011**, *43*, 668–672. [[CrossRef](#)] [[PubMed](#)]
44. Yu, M.; Liang, H.; Fu, Z.; Wang, X.; Liao, Z.; Zhou, Y.; Liu, Y.; Wang, Y.; Hong, Y.; Zhou, X.; et al. BAP1 suppresses lung cancer progression and is inhibited by miR-31. *Oncotarget* **2016**, *7*, 13742–13753. [[CrossRef](#)] [[PubMed](#)]
45. Wang, N.; Li, Y.; Zhou, J. miR-31 Functions as an Oncomir Which Promotes Epithelial-Mesenchymal Transition via Regulating BAP1 in Cervical Cancer. *BioMed Res. Int.* **2017**, *2017*, 6361420. [[CrossRef](#)] [[PubMed](#)]
46. Murata, S.; Zhang, C.; Finch, N.; Zhang, K.; Campo, L.; Breuer, E.K. Predictors and Modulators of Synthetic Lethality: An Update on PARP Inhibitors and Personalized Medicine. *BioMed Res. Int.* **2016**, *2016*, 2346585. [[CrossRef](#)]
47. Stover, E.H.; Konstantinopoulos, P.A.; Matulonis, U.A.; Swisher, E.M. Biomarkers of Response and Resistance to DNA Repair Targeted Therapies. *Clin. Cancer Res.* **2016**, *22*, 5651–5660. [[CrossRef](#)]
48. Yu, F.X.; Zhao, B.; Panupinthu, N.; Jewell, J.L.; Lian, I.; Wang, L.H.; Zhao, J.; Yuan, H.; Tumaneng, K.; Li, H.; et al. Regulation of the Hippo-YAP pathway by G-protein-coupled receptor signaling. *Cell* **2012**, *150*, 780–791. [[CrossRef](#)]
49. Ma, Y.W.; Liu, Y.Z.; Pan, J.X. Verteporfin induces apoptosis and eliminates cancer stem-like cells in uveal melanoma in the absence of light activation. *Am. J. Cancer Res.* **2016**, *6*, 2816–2830.
50. Gao, H.; Korn, J.M.; Ferretti, S.; Monahan, J.E.; Wang, Y.; Singh, M.; Zhang, C.; Schnell, C.; Yang, G.; Zhang, Y.; et al. High-throughput screening using patient-derived tumor xenografts to predict clinical trial drug response. *Nat. Med.* **2015**, *21*, 1318–1325. [[CrossRef](#)]

51. Némati, F.; Mathiot, C.; Grandjean, I.; Lantz, O.; Bordier, V.; Dewulf, S.; Ekue, R.; Di Santo, J.P.; Poupon, M.F.; Decaudin, D. Imatinib mesylate reduces rituximab-induced tumor-growth inhibition in vivo on Epstein-Barr virus-associated human B-cell lymphoma. *Anticancer Drugs* **2007**, *18*, 1029–1037. [[CrossRef](#)] [[PubMed](#)]
52. Hatem, R.; El Botty, R.; Chateau-Joubert, S.; Servely, J.L.; Labiod, D.; de Plater, L.; Assayag, F.; Coussy, F.; Callens, C.; Vacher, S.; et al. Targeting mTOR pathway inhibits tumor growth in different molecular subtypes of triple-negative breast cancers. *Oncotarget* **2016**, *7*, 48206–48219. [[CrossRef](#)] [[PubMed](#)]



© 2019 by the authors. Licensee MDPI, Basel, Switzerland. This article is an open access article distributed under the terms and conditions of the Creative Commons Attribution (CC BY) license (<http://creativecommons.org/licenses/by/4.0/>).